Mindanao Journal of Science and Technology Vol.15 (2017) 12-34

Design Study of Horizontal Axis Tidal Turbine Blade

Siddharth Suhas Kulkarni, Craig Chapman, Hanifa Shah,
Erika A. Pärn and David J. Edwards*
Department of Computing Engineering and Built Environment
Birmingham City University
Birmingham B4 7XG, United Kingdom
*david.edwards@bcu.ac.uk

Date received: July 14, 2017
Revision accepted: November 17, 2017

Abstract

A design study was conducted to understand the implications of bio-mimicking a curved caudal fin type horizontal axis tidal turbine blade design, using National Advisory Committee for Aeronautics (NACA) 0018 is presented. A method of transforming the traditional horizontal axis tidal turbine by defining a third order polynomial center line on which the symmetrical airfoils were stationed is also disclosed. Each of the airfoil characteristics: twist angle distribution, chord lengths, and a center line passing through the airfoil centers were automatically transformed to create the curved caudal fin-shaped blade; translating the spinal blade axis into percentage wise chord lengths, using NACA 0018 airfoil. A 3D mesh independency study of a straight blade horizontal axis tidal turbine modeled using computational fluid dynamics (CFD) was carried out. The grid convergence study was produced by employing two turbulence models, the standard k-ε model and shear stress transport (SST) in ANSYS CFX. Three parameters were investigated: mesh resolution, turbulence model, and power coefficient in the initial CFD, analysis. It was found that the mesh resolution and the turbulence model affect the power coefficient results. The power coefficients obtained from the standard k-ε model are 15% to 20% lower than the accuracy of the SST model. Further analysis was performed on both the designed blades using ANSYS CFX and SST turbulence model. The results between the straight blade designed according to literature and the caudal fin blade showed a maximum power coefficient of 0.4028%, and 0.5073% respectively for 2.5m/s inlet velocity.

***Keywords**:* design study, horizontal axis tidal turbine, bio-mimicry, SST turbulence model, NACA 0018

1. Introduction

Tidal energy is a renewable electricity source based on the conversion of kinetic energy of moving water into mechanical power to drive generators (Shi *et al*., 2015). It has fewer CO_2 emissions, and it has minimal reliance on fossil fuels. It is one of the many sources to address concerns over climate change (Tedds *et al*., 2014). As there is a need to identify and use more sustainable sources of power generation tidal energy will gain more attention. Tides result from the gravitational pull of the moon. As 71% of the earth's surface is covered by water, energy can be harnessed on a large scale through tides (Blunden and Bahaj, 2006). Tides are predictable, which is also the greatest advantage that tidal energy has over other renewable sources like wind or solar power.

Horizontal axis tidal turbines (HATT) are also known as axial flow turbines; they have the rotational axis parallel to the tidal flow; thus, they operate in only one flow direction. The principle of operation of the HATT is similar to the horizontal axis wind turbine (HAWT); it has blades fitted to the hub, a generator to convert kinetic energy from the water to mechanical energy, shaft to produce power and gearbox (Bai *et al*., 2016). There have been many advances in the development of the computational power and computational fluid dynamics (CFD) models to simulate the complex flow around the turbine (Malki *et al*., 2014).

Some relevant studies on mesh independency techniques exist to improve the accuracy of the CFD simulations. The independent mesh solutions are entirely dependent on the mesh selected to resolve the fluid flow and the turbulence model that is chosen to illustrate the physics of the problem. The characteristics of a 10m diameter three-bladed HATT and the mesh was generated using ANSYS ICEM CFD (12C x 20C rectangular grid), which was very fine near the blade wall region to obtain precise results, but no y+ values were given in the source (Goundar and Ahmed, 2013). The authors found that by varying the thickness of the airfoil the hydrodynamic performance, as well as the strength of the blade, was good with the rotor producing a maximum efficiency of 47.6%. Another study, based on the mesh dependency of a tidal turbine blade, was performed by analyzing the wake performance in non-uniform flow using the k-ε turbulence model and demonstrating using the two different profiles with the same coarse mesh settings. This produced small changes in the power coefficients of the two different rotors (Masters *et al*., 2013). A numerical investigation and calibration of SST turbulence model were carried out to test the operational

performance of a small-scale horizontal axis wind turbine (SS-HAWT). The grid sensitivity analysis exhibited the y+ of less than 5, including the blade tip to eliminate the discretization error from the solution, and thus reduce the computational burden (Rocha *et al*., 2014). Four numerical techniques, i.e., grid convergence index (GCI), the fitting method, mesh refinement and General Richardson Extrapolation (GRE), were carried out to produce a mesh separated solution and for VAWT and to generate a power curve using CFD (Almohammadi *et al*., 2013). The CFD solution was produced using two turbulence models, SST and RNG k- ϵ. They achieved the mesh independent solution after converging the mesh solution and examining the iterative convergence error. Thrust and power coefficients of a 3D CFD tidal turbine model were validated with the experimental data especially at 15° and 20° of pitch angle and had a good agreement. The authors analyzed the tidal turbine pressure, and near-wall effects were ANSYS's Shear Stress Transport (SST) also considering the mesh resolution and time step convergence (McSherry *et al*., 2011).

As the west coast of Korea experiences adamant tidal currents with up to 10m in tidal range; Jo *et al*., (Jo *et al*., 2014) designed a horizontal axis tidal turbine based on BEM and calculated its efficiency performance to be 40% choosing five as the tip speed ratio. They also investigated the wake distribution in the unsteady velocity flow affecting the tidal turbine system. The CFD analysis was performed using the SST turbulence model, and the curves of C_P and torque generated from the shaft were presented for different velocities. Batten *et al*., (Batten *et al*., 2007) carried out a study based on analyzing total power output cavitation aspects of a horizontal axis tidal turbine which was scaled down to the $1/20^{th}$ model of the actual 16 m diameter rotor. They also compared the cavitation tunnel experimental data with the blade element theory model which was used to obtain the axial flow factors on the turbine. They concluded with developing an optimization program which maintains design speeds for the analyzed turbine.

Biomimicry or biomimetics has proved to be an excellent motivation to solve complex human problems, by imitating nature. The design process starts by looking at nature's ecosystem, self-healing abilities or a particular organism, to produce a design solution to the human need. The classic example of the bio-mimicry is the Humpback Whale wind turbine, designed adapting the whale's flippers and tubercles (Fish *et al*., 2011; Fish and Battle, 1995; Shi *et al*., 2016). The locomotion of the marine vertebrate is based on the five fins namely; caudal, anal, pelvic, pectoral, and dorsal fins which are located around its body, and the movements caused because of

these flexible fins act as the primary source for propulsion at high swimming efficiency. As 80% of the propulsive efficiency, i.e., the swimming speed, e.g. Blue Marlin fish is caused due to its high lift generating caudal fin, which makes it one of the fastest propelling fishes under the ocean, and also enables it to be efficient even at the low velocities).

This paper aims to introduce a new design based on bio-mimicking curved caudal fin for the CFD analysis of HATT blades. A mesh independency of a straight blade HATT is carried out, by employing two turbulence models namely the standard k-ε model and SST model, to keep the computational costs low. The grid convergence study was performed by developing three different meshes: with a coarse, medium, and fine grid for all six different meshes of the straight blade to predict the power, lift coefficients, and torque on normalized mesh cells to determine how the mesh quality affects CFD simulation results. Furthermore, an original caudal fin-based geometry characterized with symmetrical airfoil distribution, and the caudal fin-shaped blade produces higher efficiency throughout the year, i.e., even for the lower tidal flow velocities which occur during the winter months. Therefore, the overall power coefficient of the designed caudal fin-shaped blade is higher throughout the season.

2. Methodology

2.1 Determination of the Blade Parameters

Figure 1 shows a NACA airfoil traditionally used to design tidal turbine blades. In the tidal turbine industry, both symmetrical and asymmetrical airfoils are used to create HATT (Etemadi *et al*., 2011). Symmetrical airfoils due to the angle of attack variation over the full turbine blade rotation and the high cavitation properties are most popular in the tidal turbine design (Liu and Veitch, 2012). Previous examples of the use of symmetrical airfoils in tidal turbine blade design can be found in Masters *et al.*, (Masters *et al*., 2013), and Yang & Shu (Yang and Shu, 2012). These airfoils travel in a tangential direction in the axial path of the tidal current flow, and hence, the airfoil chord length is not parallel to the flow as is that of VATT, but traveling across it. As the fluid velocity increases over the airfoils, the convex surface results in lower pressure on the suction side when compared to the pressure side of the airfoil. Therefore, symmetrical airfoils to modeling a bio-mimicked HATT blade have not been in tidal energy

generation. The caudal fin blade design; NACA 0018 was chosen to model both HATT's, as the seawater velocity increases over the increasing angle of attack of the upper surface of the airfoils resulting in higher drag forces when a HATT completes a full rotation, and also causing lift fluctuations. Therefore, designing a blade like a curved caudal fin generates higher lift and power coefficients at both lower and higher tidal current velocities with less vibration.

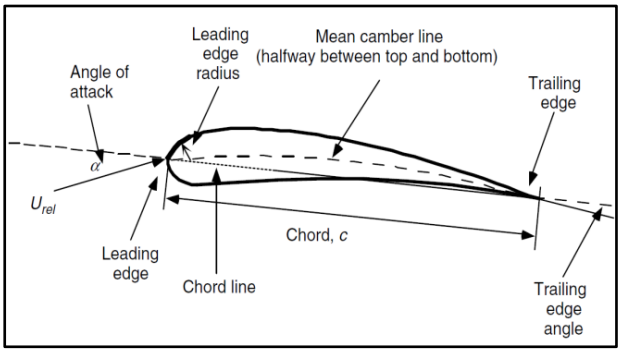

Figure 1. Airfoil characteristics (Bavanish and Thyagarajan, 2013)

2.2 Parametric Design Study

The parametric study intended to determine a traditional HATT (referred as a straight blade in this paper), before designing the caudal fin-shaped blade. The top-level design parameters that define the three-dimensional straight blade are blade height, total blade height, symmetrical airfoils, and twist angle distribution as shown in Figure 2. The spanwise distribution of the airfoils is done at every 10% of the blade. The distance between hub circle and the root airfoil is 20% of the total blade radius (R). The diameter of the hub circle is 40% of the root airfoil chord length. E.g., if the root airfoil chord length is 1000mm, then the hub circle diameter would be 400mm (the hub circle is a cylindrical surface which is lofted with the root airfoil). After defining the default value of the root airfoil chord length (1000mm), the remaining airfoil chord length distribution is done using a constant reduction factor of 0.08R, which is termed The Blade chord length reduction factor and is used to calculate the chord lengths of remaining airfoils. The rotor diameter is also a design variable which is retrieved at the theoretical design phase of the tidal turbines together with the number of blades, hub and nose height, diameter.

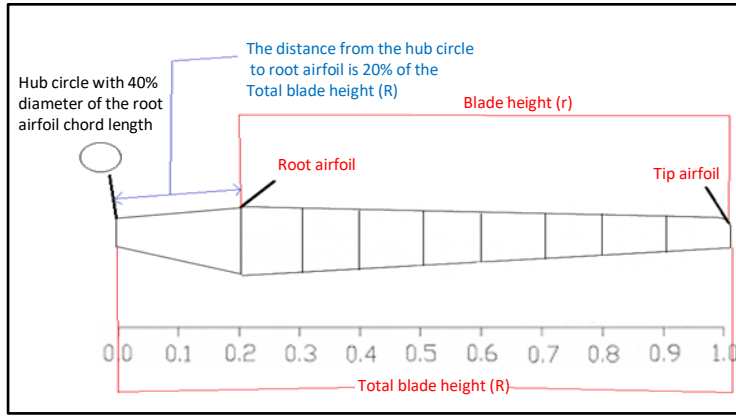

Figure 2. Blade span airfoil distribution

As shown in Figure 3, a top plan view of the twist angle is defined on all the airfoil stations. The blade twist angle is higher at the root airfoil because it experiences fewer rotational forces on the blade and it gradually starts decreasing towards the entire span of the blade. As the angular velocity of the blade is highest on the tip of the blade, the twist angle is at least four times smaller than the root airfoil twist angle. After determining the parameters mentioned above, the rotor span was fixed. Then, the airfoil, chord length, and the twist angle distribution were defined as shown in Table 1.

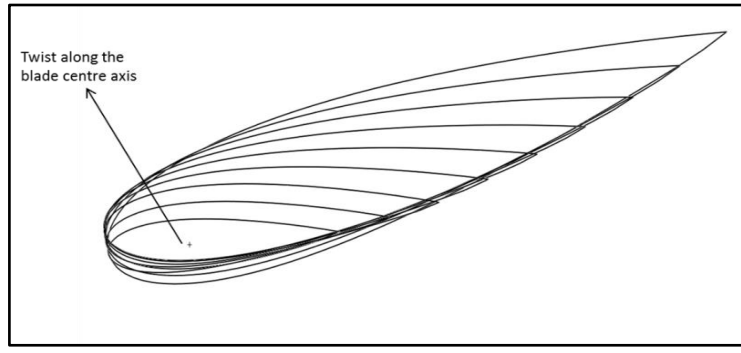

Figure 3. NACA airfoils twisted about the central axis of blade

Table 1. Parametric blade design study

R (mm)	Chord length, c (mm)	Twist distribution (°)	NACA airfoil
1410	1000	16	0018
1970	920	14	0018
2530	840	12	0018
3090	760	10	0018
3660	680	8	0018
4220	600	6	0018
4790	520	4	0018
5320	440	4	0018
5920	360	4	0018

2.2 Locomotion and Anatomy of the Marine Vertebrates

The caudal fin propulsion may represent a ship is rudder at high speed, or an airplane movement operating with the same forces like pitch and thrust, including the transfer mechanisms like drag and lift (Figure 4). The locomotion of the marine vertebrates, e.g. the Blue Marlin fish, *Makaira nigricans* whose swimming speed has been recorded up to 80 km/h (50 MPH) is based on the five fins namely; caudal, anal, pelvic, pectoral, and dorsal fins. Thus, these marine vertebrates employ thrust maneuvering, or in other words, they use their fins for the propulsion (Lenarz and Nakamura, 1972). The pectoral and pelvic fins contribute to the maneuverability to swim at low-velocity marine currents, with the caudal fin creating the essential thrust for propulsion (Tokić and Yue, 2012). The caudal fin propulsion may represent a ship's rudder at high speed, or an airplane movement operating with the same forces as pitch and thrust, including the transfer mechanisms of drag and lift. The pressure related forces drag and lift originate due to the inequality of the water flow acting on the fish body. This propulsion is also termed as the Body and Caudal Fin (BCF) propulsion (Wilga and Lauder, 2001), which may cause surface area increment or decrement; thus, the swimming movements may differ from species to species. The dorsal fins protect the fish from rolling and help in turning, thus controlling the body at low speeds or to a complete stop (Jayne *et al*., 1996). The anal fins are located ventrally in the anus region of the fish and help to manage the body orientation to maintain stability when the swimming velocity increases (Zhou *et al*., 2008). The caudal fin, which is also termed the tail fin, is located at the end of the fish's body (caudal penuckle) and is

the main fin that produces thrust propulsion through seawater (Windsor *et al*., 2010). The propulsive efficiency of the Blue Marlin ranges in between "0.85 to 0.91%" (Block *et al*., 1992; Luthy *et al*., 2005).

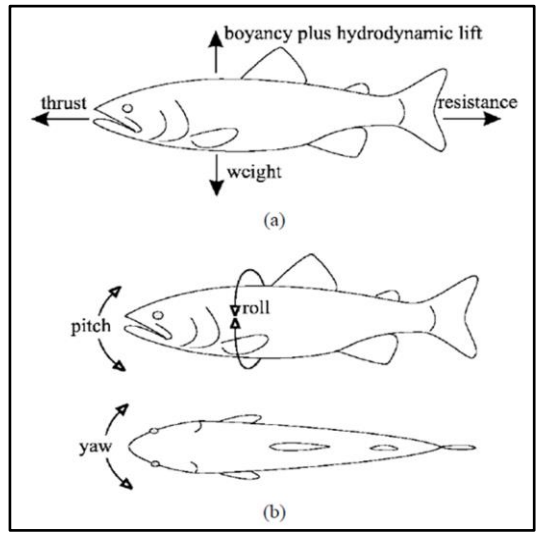

Figure 4. The locomotion forces acting on the fish while swimming (Sfakiotakis *et al*., 1999)

2.3 Moving the Center Line and Chord Length Variation

The 3D curved a set of centroids characterizes caudal fin blade; a MATLAB program was created in which the centroids of the NACA airfoil centers form a 3D shape as predicted by the MATLAB program. The MATLAB program computes the center of mass (gravity) for the set of airfoils used in modeling the curved caudal fin blade. The weighted centroid uses the pixel intensities in the airfoil region which weights in the centroid calculation. NACA 0018 is a symmetrical four digit airfoil, and center of mass lies on the line of symmetry, and it has a homogeneous center of the mass distribution. The airfoil stations were induced to rotate freely around its center of mass due to the hydrodynamic forces under the action of an incompressible seawater flow. The 3D curved caudal fin shape generated from the Matlab program is reproduced below (see Figure 5).

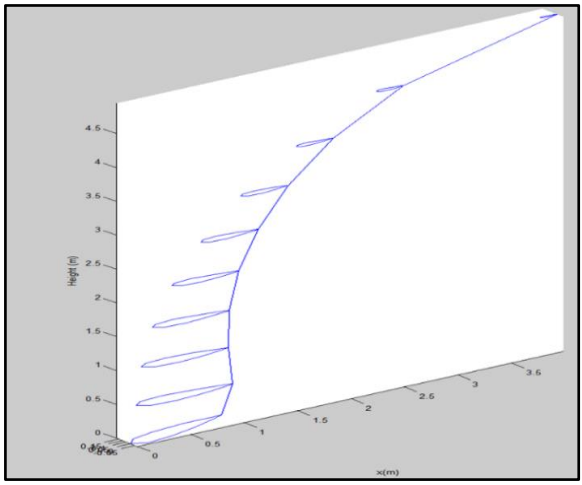

Figure 5. A three-dimensional plot of the curved caudal fin blade reproduced by MATLAB program.

The twist angle which acts as the function of the incremental blade length is further modified by to create a smooth twist by fitting a third order polynomial function. To (or "intending to") getting the desired curve for the initial tidal turbine blade to move towards the curved caudal fin shape (the target shape), a third order polynomial function is defined on the central axis curve. Thus, for programming, the nearest third order polynomial equation is defined below using polynomial regression analysis in MS-Excel and is demonstrated in Figure 6.

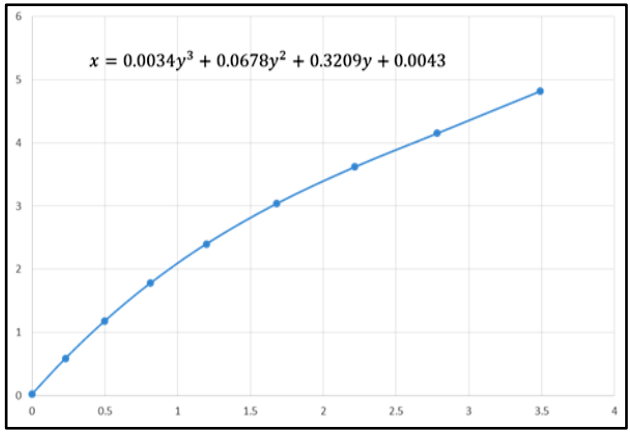

Figure 6. The skeleton (center line) of the caudal fin-shaped blade fitted with third order polynomial function.

The third order polynomial function is defined on the central axis curve is:

$$x = 0.0034y^3 + 0.0678y^2 + 0.3209y + 0.0043 \quad (1)$$

The above equation is considered to be the center line polynomial function of the curved blade caudal fin. Each NACA profile center is built on the center line, the center line then acts as a master and each profile datum sits along its length divided by the height and the numbers of stations stay constant as the default straight blade. Using this approach, it would be easy to model the curved shape blade and hence reduce the computational overhead. All the NACA profile sections are considered parallel to the x-axis, i.e., the normal of each NACA section should be the y-axis. The skeleton which is fitted on the midpoint of each airfoil has a decrease in the chord length in the blade spanwise direction which increases the surface area of the caudal fin-shaped blade. Fitting the third order polynomial on the skeleton of the caudal fin looks like centreline, starting at the airfoil root center and passing through all the airfoil stations to the tip airfoil center entails the blade bending and thus creates the caudal fin-shaped blade.

The chord lengths of the straight blade can be varied in linear or non-linear progression along the spanwise direction to reach the caudal fin-shaped blade as shown in Figure 7. The caudal fin-shaped blade also has a thicker base than the straight blade to mount on the rotor without having to use additional support. The blade twist is also varied along all the airfoil stations making the caudal fin-shaped blade produce more energy from the tidal currents. This is particularly suitable for the caudal fin-shaped blade because of the increasing concave bend and thinness at the tip and thus, should be dimensioned to have sufficient strength at the tip of the blade. The most important design variables that affect the overall efficiency of the horizontal axis tidal turbine system are chord lengths of airfoils, twist distribution, the overall height of the blade, the angle of attack, the angular velocity of the blade, blade material, and the fluid velocity acting on the blade (Afgan *et al*., 2013; Betz, 2014; Clancy, 1975; Mycek *et al*., 2013; Pinon *et al*., 2012). The design variables selected to move the straight blade towards the caudal fin-shaped blade are airfoil chord lengths, the total blade height, and twist angle distribution; however, the other important design variables that construct a HATT are outside of the scope of this paper.

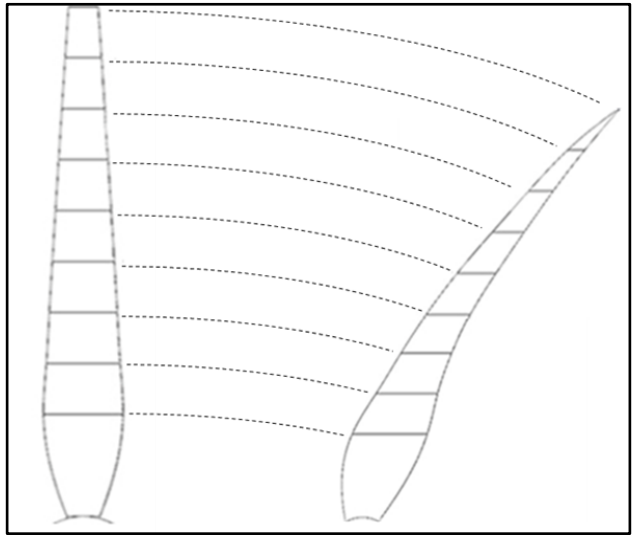

Figure 7. Chord length variation of the straight blade to achieve caudal fin-shaped blade

2.4 CFD Simulation Setup

As mentioned in the previous sections NACA 0018 was employed on both the designed blades. This paper compares the non-dimensional forces lift, power coefficients and their variations produced by SST turbulence model, at the turbine level thus putting forward a comparative analysis.

2.4.1 Meshing, Boundary Conditions, and Turbulence Model

Figure 8 shows the rectangular computational grid which was used to model the seawater domain and the turbine disc domain, for the straight blade and caudal fin-shaped blade geometries. The seawater domain extends 5 times the turbine diameter at the inlet and 10 times of the turbine diameter at the outlet, and the height of the rectangular grid is five times of the turbine diameter. The turbine domain was designed as rotating domain in CFX, and then a full 360° mesh surrounding the tidal turbine blades. An unstructured tetrahedral mesh was constructed around this domain as the flow would be highly non-linear, and the rotational effects are to be considered. Figure 9 shows blade automated meshing including the hub and tips of the straight blade and the caudal fin-shaped blade.

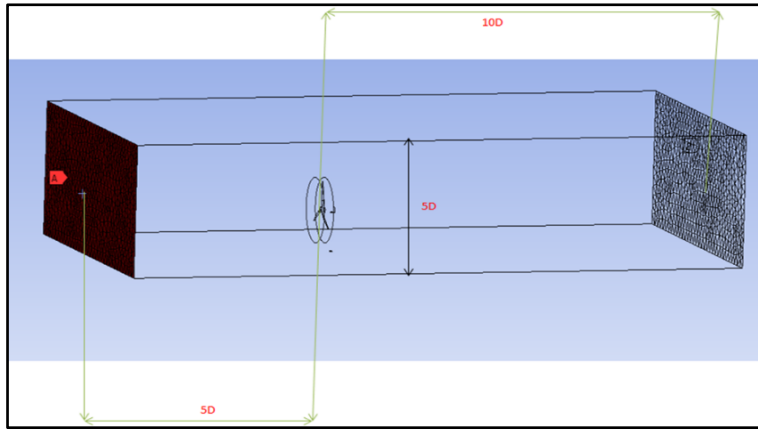

Figure 8. Inlet, outlet, and height extension from the turbine blades

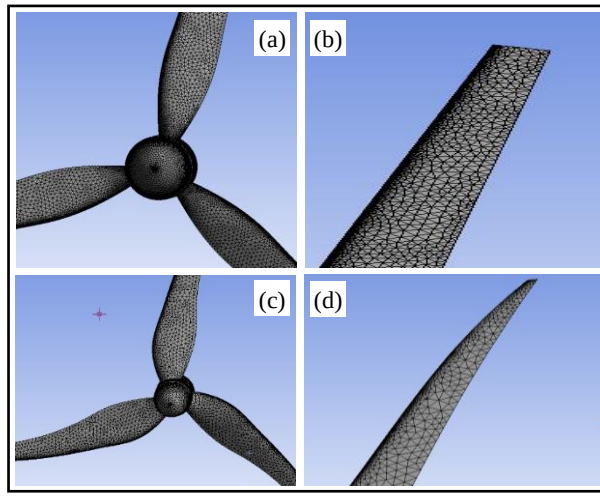

Figure 9. (a) Meshed straight blade with blades and hub, (b) straight blade meshed tip, (c) meshed fin blade with blades and hub, and (d) caudal fin blade meshed tip

In the meshing aspect, the tetra-prism mesh consisted of 151740 nodes and 252839 nodes for the straight blade and caudal fin blade case studies respectively, including the turbine disc rotating domain. The three-dimensional modeling and steady-state CFD simulations presented in this paper are conducted using ANSYS CFX, the fluid was defined as seawater and was simulated at constant inlet velocity of 2.5m/s, using high turbulence intensity of 10%. The outlet pressure was defined as 0bar, the blade was

intensity of 10%. The outlet pressure was defined as 0bar, the blade was defined as a rotating wall, with no slip wall condition, for mass and momentum option. The bottom and side walls were defined as the free slip walls to incorporate the accuracy when solving the continuity equation. The front and back walls were defined as inlet and outlet walls respectively.

2.4.2 Standard K-Epsilon (k-ε) Turbulence Model

The k-epsilon (k-ε) turbulence model is the most widely used in CFD to analyze and simulate the turbulent flow conditions. It is a two-equation turbulence model as it describes the result for conservation equations using two transport equations k and epsilon. This model is an improvement to the mixing length model as it has good stability for high Reynolds number turbulent flow (Launder *et al*., 1975). The first transport model k-equation arbitrates the energy from the turbulent kinetic energy equation and is described as turbulent kinetic energy (k). The second transport model is the dissipation of turbulence (ε), which describes the rate at which turbulent kinetic energy dissipates. The experimental form for the standard k-ε model can be described as (Wilcox, 1998):

$$\frac{\partial(\rho k)}{\partial t} + \nabla.(\rho k\bar{u}) = \nabla\left[\frac{\mu_t}{\sigma_k}\nabla.k\right] + P - \rho \quad (2)$$

$$\frac{\partial(\rho \epsilon)}{\partial t} + \nabla.(\rho \epsilon\bar{u}) = \nabla\left[\frac{\mu_t}{\sigma_\epsilon}\nabla.\epsilon\right] + C_{1\epsilon}\frac{\epsilon}{k}P - C_{2\epsilon}\,\rho\frac{\varepsilon^2}{k} \quad (3)$$

Where u s is the velocity component in a parallel direction, E_{ij} is the rate of deformation, $\mu_t = C_\mu \rho \frac{k^2}{\epsilon}$ is the eddy viscosity and $P = 2\mu_t S_{ij}.S_{ij}$

2.4.3 Shear Stress Transport (SST) Turbulence Model

The SST model was developed by (Menter, 1993); it assimilates the inner and outer region of the boundary layer in between the eddy viscosity and full turbulent viscosity formation. The SST model draws up the best effects of k-ε (accurate precision of results in the far field region) and k- ω (good accuracy in providing results in the near wall region), it being used as low Reynolds number model without any blending functions changes the cross term function) also prevents being too sensitive to inlet free stream turbulence.

$$\frac{\partial(\rho\omega)}{\partial t} + \nabla.(\rho\omega\bar{u}) = \nabla\left[\mu + \frac{\mu_t}{\sigma_{\omega,1}}\nabla.\omega\right] + \gamma_2\left(2\rho S_{ij}.S_{ij} - \frac{2}{3}\rho\omega\frac{\partial\bar{u}_i}{\partial x_j}\delta_{\square j}\right) - \beta_2\rho\omega^2 + 2\frac{\rho}{\sigma_{\omega,2}\omega}\frac{\partial k}{\partial x_k}\frac{\partial\omega}{\partial x_k} \quad (4)$$

The SST turbulence model was chosen to predict the accurate hydrodynamic flow and pressure gradients on the airfoil, and also because of its good prediction of the boundary layer separation. The calculations were performed with an Intel (R) Xeon (R) [3.30GHz*2]. The convergence condition was determined in a margin error less than 10^{-5}, and simulating each case study required at least three hours.

2.5 Mesh Indepedency Study

To establish the accuracy of the CFD solution, and to keep the computational costs low, the straight blade was analyzed using: the standard k-ε model, and SST model, at uniform V_{in} = 2.5m/s, and λ = 5. The grid convergence study was performed by developing three different meshes: with a coarse, medium, and fine grid for all six different meshes of the Straight Blade to predict the power, lift coefficients, and torque on normalized mesh cells to determine how the mesh quality affects CFD simulation results.

The number of nodes and the simulation time for the three cases simulated using the SST model are highlighted in Table 2, and the three cases simulated using the standard k-ε model are given in Table 3. Table 2, and 3 summarise the key characteristics of the meshes, and it is very clear that CFD simulation time is highly dependent on the number of mesh nodes considered. The six meshes generated have near wall resolution, i.e., y+ < 10 by using the standard wall function approach to avoid unsatisfactory results when using the standard k – ε model.

Table 2. Mesh size, CFD simulation time, and estimated C_P for SST model at λ = 5

Mesh Resolution	Coarse Mesh (M1)	Medium mesh (M2)	Fine mesh (M3)
Number of nodes	79859	151740	230439
CFD simulation time	4hrs 10mins	6hrs 16mins	9hrs 53mins
Estimated C_P	0.3816	0.4169	0.4218

Table 3. Mesh size, CFD simulation time, and estimated C_P for k-ε model at $\lambda = 5$

Mesh Resolution	Coarse Mesh (M4)	Medium Mesh (M5)	Fine Mesh (M6)
Number of nodes	44064	92767	139506
CFD simulation time	1hr 36mins	4hrs 41mins	5hrs 38mins
Estimated C_P	0.2271	0.2586	0.2693

In the case of the investigated meshes of the straight blade, the turbine domain has an increased mesh resolution due to the blades being exposed to the complex flow separation. The mesh is refined in the grids from M1 to M6 where M1, M2, M3 represent coarsely, medium, and fine mesh generated for the SST turbulence model; and M4, M5, M6 represent coarse, medium, and fine mesh generated for the standard k-ε turbulence model. The estimated power coefficient increased from 0.2271 to 0.4218 as shown in Figure 10.

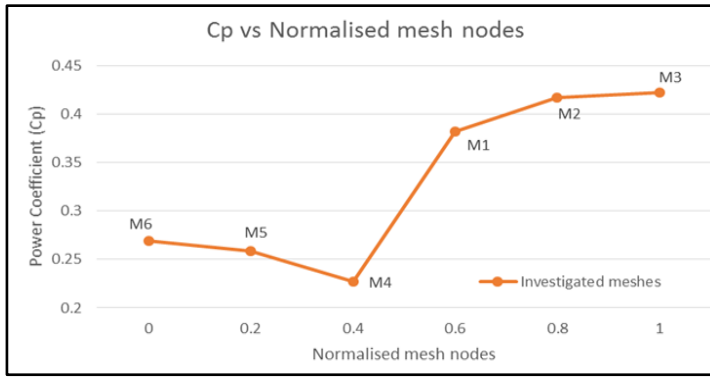

Figure 10. The power coefficients of all the investigated meshes independecy study

It is important to note that the mesh resolution plays a pivotal role in the final CFD results. The mesh nodes need to be small to resolve the boundary layer on the blade surfaces. The highest CP obtained from the independent mesh study is 0.4218 for M3 from the SST model. M2 and M3 account for nearly 1% difference in the estimated power coefficients, but the final CFD simulation time required for convergence of the two meshes has a significant difference when the conventional mesh independency method is employed. The power coefficients obtained from the standard k-ε model are almost 15% to 20% lower than the SST model power coefficients, which is due to the poor performance of the k-ε model in near-wall regions and adverse pressure gradients i.e. the fluid flow near the turbine blade surfaces; which causes the k-ε model to underestimate the power coefficient.

It is clear from the final CFD simulation results that the simulation time is highly dependent on the number of mesh nodes, and the turbulence model selected. As shown in Figure 10 when using k-ε model for all the meshes (M4, M5, and M6) employed the CFD solution under predicts power coefficient when compared with the SST model. M1 leads to the reasonable prediction of the power coefficient on the straight blade, whereas the power coefficient of M3 is slightly better than M2. Due to the slight difference medium mesh (M2) is best regarding computational costs and is further employed for the numerical analysis carried out in the following section of the turbulence model comparison study.

2.6 Turbulence Model Comparison Study

To understand the sensitivity of the CFD solution a consecutive study was carried out with these turbulence models at medium sized meshes. From the mesh dependency test conducted it has been found that the SST model performs superiorly in adverse pressure gradient situations than the standard k-ε model; because SST model is a unification of k-ε model and k-ω model for free stream and inner boundary layer problems respectively. Figure 11 shows the torque coefficient related to each of the two turbulence models analyzed for the medium mesh. As shown in Figure 4 the SST model medium mesh has higher CM than the standard k-ε model in all the nine different TSR's. It can also be seen that the torque coefficient of SST medium mesh model increased by more than 25% when compared to the standard k-ε model medium mesh.

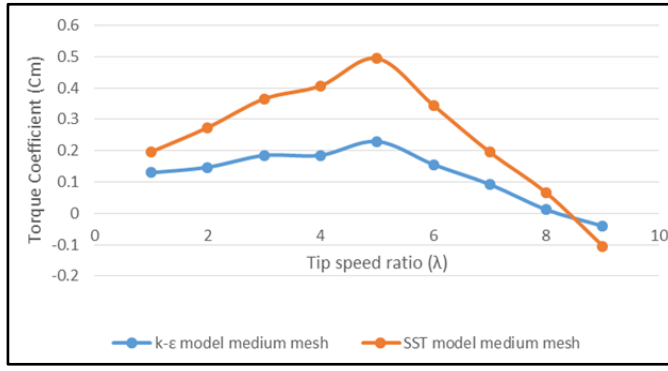

Figure 11. Torque coefficient versus tip speed ratio k-ε and SST model medium meshes

The highest CM is achieved at λ= 5 for both the cases, CM increases with the increasing TSR and acts as a function of TSR. It can also be noted that the non-linearity in the torque coefficient occurs after TSR of 5, and the k-ε model fails to capture this, due to the boundary layer and turbulence quantities to the blade wall.

Figure 12 shows that the power coefficient increases steadily until TSR ≈ 5, at which it shows the peak CP ≈ 0.4169 for the SST model medium mesh; after which it shows a drastic reduction with the increasing λ > 6. The curve for medium mesh the k-ε model shows that it predicts a lower power coefficient to a satisfying level of accuracy, and also underpredicts the values with increasing λ. However, the numerical CP prediction by medium mesh the SST model observed values are approximately 20% higher than medium mesh the k-ε model simulation, the range $5 \leq \lambda \leq 6$ was also validated (Bahaj *et al*., 2007; McSherry *et al*., 2011); and considered to be optimum range for HATT. The standard k-ε model is incapable of capturing the account of rotational forces and their effects on the turbine blades, and due to the near wall physics implementation. Thus the CP prediction by SST model is more acceptable when compared to the power coefficient predictions by the standard k-ε model.

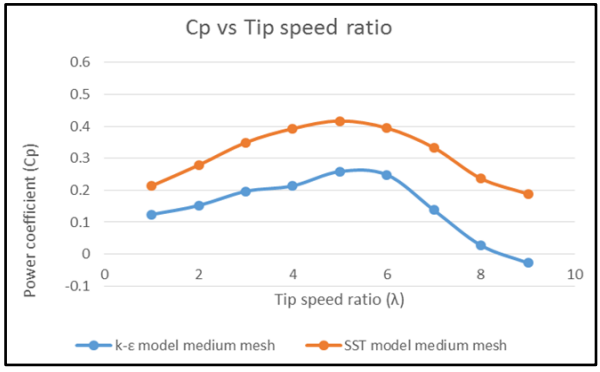

Figure 12. Power coefficient versus tip speed ratio for k-ε and SST model medium meshes

As a result of the mesh independency test conducted, it can be concluded that the overall power coefficient shown by the SST turbulence model is more reasonable than the standard k-ε model, for all the cases considered. Therefore, to avoid any misleading CFD results the standard k-ε model is not employed in any further CFD tests conducted in this research. The power coefficient of a HATT is highly sensitive to the turbulence model chosen for

the CFD analysis; however, the mesh independent CFD solution for SST medium mesh satisfactorily achieves the mesh independency over the SST fine mesh solution which requires a massive computational overhead. Hence, the medium mesh is used to conduct the steady-state analysis in following sections.

3. Results and Discussion

As the seawater flow velocity progressed over the blade pressure side, the pressure increased especially on the tip of the blade as it was affected due to the rotational velocity being the highest on the tip. At the same time, flow velocity decreased; which further resulted in rigorous movements on the blade suction surface except on the trailing edge of the blades. Figure 13 shows the comparison of the blade pressure distribution on the case studies performed.

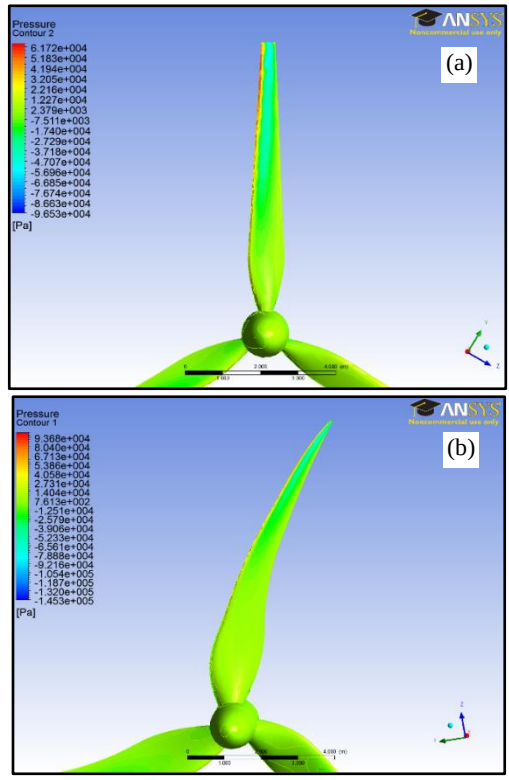

Figure 13. Blade pressure distributions (pressure side) on a) Straight blade and b) Caudal fin-shaped blade.

The above figure compares the steady-state pressure distribution on the two blade designs. The numerical simulations show how the seawater flow behaves on the trailing and the leading edge on the pressure side of the blade. It can also be seen that the positive blade tip vortex is seen on the pressure side of the blade and the negative blade tip vortex is produced on the suction side of the blade. This is because of the high turbulence intensities generated from the trailing edge of the airfoil and thus creating downstream interaction of the Reynolds shear stress and turbulent boundary layer formation. The NACA 0018 airfoil, a high lift generating airfoil, generates lift from the pressure difference created by the fluid and blade interaction. Figure 14 shows blade rotational velocity and streamlines on the two case studies performed. It can be seen that the fluid velocity increases as it passes through the turbine causing it to produce higher efficiency.

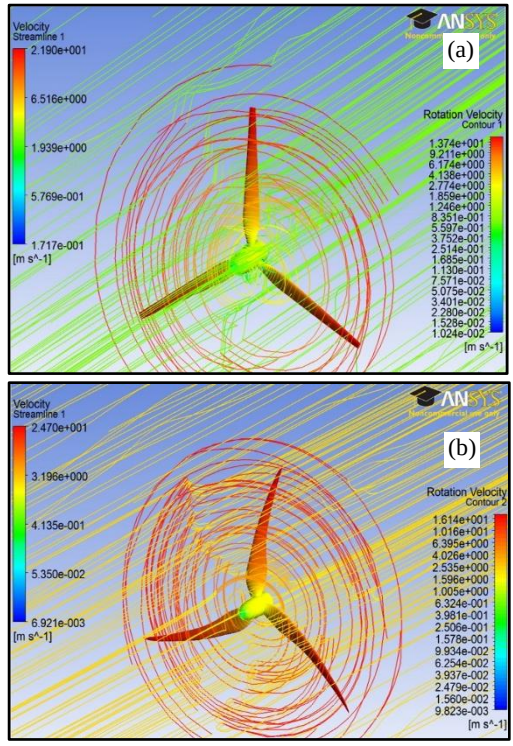

Figure 14. Steady-state blade rotational velocity streamlines for a) straight blade and b) caudal fin-shaped blade

After comparing the blade pressures of the straight blade and, the pressure prediction on the tip of the blade where the rotational velocity of the blade is at its highest also causing higher lift on the pressure side of the blade, and also risking the chances of facing cavitation. It also further shows that the region most affected by the seawater is the tip chord of the blade along with its leading and trailing edge, due to the unsteady vibrations of the blade which are highlighted by SST. The straight blade produces 366 kW of power, and power coefficient of 0.4028% while curved caudal fin-shaped blade produces 435 kW and a power coefficient of 0.5073%.

4. Conclusions

This study investigates the efficacy of blade design by bio-mimicking a caudal fish fin for a tidal current power turbine. A default horizontal axis tidal turbine was designed according to the literature termed as Straight Blade in this paper, with a diameter of 14.2m using NACA 0018 airfoil. The turbine blade level parameters total blade radius, twist rule, and NACA airfoil was demonstrated. A third order polynomial function was introduced on the centreline which passed through the airfoil centers to design the caudal fin-shaped blade, by varying the airfoil chord lengths. A mesh independency study of a straight blade to determine the mesh sensitivity and its effects on the CFD simulation results. The grid convergence study was simulated using two turbulence models: the standard k-ε model, and SST turbulence model at coarse, medium, and fine mesh resolution thus simulating six different mesh sizes. This paper has shown that obtaining independent mesh solutions is a fundamental need for all the tidal turbine blade designers due to the sensitivity of the lift coefficient of the tidal turbine.

The standard k-ε model under predicts the power coefficients and the simulation time is highly dependent on the mesh and turbulence model chose for CFD analysis. The highest CP obtained from the independent mesh study conducted is 0.4218 for M3 from SST model and the lowest CP 0.2693 for M6 using k-ε model. M2 and M3 account for nearly 1% difference in the estimated power coefficients, but the final CFD simulation time required for convergence of the two meshes is substantially different when conventional mesh independency method is employed. At the inlet velocity, 2.5m/s the maximum power coefficient was 0.4028% for the straight blade and 0.5178% for the caudal fin blade. The meshing of the caudal fin blade proved problematic due to bend on the blade. This was overcome by

dividing the blade into sections and producing section-by-section meshing. The steady state pressure distribution showed pressure rise from mid-section to the tip of the blades and upstream pressure being higher on the leading edge in both the cases; and proves pressure distribution is a predominant output for determining the lift and power coefficients. Thus, it can be proved that bio-mimicking a caudal fin look alike turbine blade, i.e., caudal fin blade produces greater efficiency than the default straight blade which was designed according to the tidal turbine blade literature, and meets the objectives of this paper.

5. References

Afgan, I., McNaughton, J., Rolfo, S., Apsley, D.D., Stallard, T. and Stansby, P., (2013). Turbulent flow and loading on a tidal stream turbine by LES and RANS., International Journal of Heat and Fluid Flow, Elsevier, Vol. 43, pp. 96–108.

Almohammadi, K.M., Ingham, D.B., Ma, L., and Pourkashan, M., (2013). Computational fluid dynamics (CFD) mesh independency techniques for a straight blade vertical axis wind turbine., Energy, Elsevier, Vol. 58, pp. 483–493.

Bahaj, A.S., Molland, A.F., Chaplin, J.R., and Batten, W.M.J., (2007). Power and thrust measurements of marine current turbines under various hydrodynamic flow conditions in a cavitation tunnel and a towing tank., Renewable Energy, Elsevier, Vol. 32 No. 3, pp. 407–426.

Bai, G., Li, W., Chang, H. and Li, G., (2016). The effect of tidal current directions on the optimal design and hydrodynamic performance of a three-turbine system., Renewable Energy, Elsevier, Vol. 94, pp. 48–54.

Batten, W.M.J., Bahaj, A.S., Molland, A.F., Chaplin, J.R., Group, S.E.R., and others, (2007). Experimentally validated numerical method for the hydrodynamic design of horizontal axis tidal turbines., Ocean Engineering, Elsevier, Vol. 34 No. 7, pp. 1013–1020.

Bavanish, B. and Thyagarajan, K., (2013). Optimization of power coefficient on a horizontal axis wind turbine using bem theory., Renewable and Sustainable Energy Reviews, Elsevier, Vol. 26, pp. 169–182.

Betz, A., (2014). Introduction to the Theory of Flow Machines, Elsevier.
Block, B.A., Booth, D. and Carey, F.G. (1992), “Direct measurement of swimming speeds and depth of blue marlin., Journal of Experimental Biology, The Company of Biologists Ltd, Vol. 166 No. 1, pp. 267–284.

Blunden, L.S., and Bahaj, A.S., (2006). Initial evaluation of tidal stream energy resources at Portland Bill, UK., Renewable Energy, Elsevier, Vol. 31 No. 2, pp. 121–132.

Clancy, L.J., (1975). Aerodynamics, Pitman Aeronautical Engineering Series., Pitman Publishing, London, John Wiley & Sons, New York.

Etemadi, A., Emami, Y., AsefAfshar, O., and Emdadi, A. (2011). Electricity generation by the tidal barrages., Energy Procedia, Elsevier, Vol. 12, pp. 928–935.

Fish, F.E., and Battle, J.M., (1995). Hydrodynamic design of the humpback whale flipper., Journal of Morphology, Wiley Online Library, Vol. 225 No. 1, pp. 51–60.

Fish, F.E., Weber, P.W., Murray, M.M., and Howle, L.E., (2011). The tubercles on humpback whales' flippers: application of bio-inspired technology., Integrative and Comparative Biology, Soc Integ Comp Biol, Vol. 51 No. 1, pp. 203–213.

Goundar, J.N., and Ahmed, M.R., (2013). Design of a horizontal axis tidal current turbine., Applied Energy, Elsevier, Vol. 111, pp. 161–174.

Jayne, B.C., Lozada, A.F., and Lauder, G.V., (1996). Function of the dorsal fin in bluegill sunfish: motor patterns during four distinct locomotor behaviors., Journal of Morphology, Philadelphia, Pa.: Wistar Institute of Anatomy and Biology,[1931-, Vol. 228 No. 3, pp. 307–326.

Jo, C.-H., Lee, J.-H., Rho, Y.-H., and Lee, K.-H., (2014). Performance analysis of a HAT tidal current turbine and wake flow characteristics., Renewable Energy, Elsevier, Vol. 65, pp. 175–182.

Launder, B.E., Reece, G.J., and Rodi, W., (1975). Progress in the development of a Reynolds-stress turbulence closure., Journal of Fluid Mechanics, Cambridge University Press, Vol. 68 No. 3, pp. 537–566.

Lenarz, W.H., and Nakamura, E.L., (1972). Analysis of length and weight data on three species of billfish from the western Atlantic Ocean., Proceedings of the International Billfish Symposium, Kailua-Kona, Hawaii, pp. 9–12.

Liu, P., and Veitch, B., (2012).Design and optimization for strength and integrity of tidal turbine rotor blades., Energy, Elsevier, Vol. 46 No. 1, pp. 393–404.

Luthy, S.A., Cowen, R.K., Serafy, J.E., and McDowell, J.R., (2005). Toward identification of larval sailfish (Istiophorus platypterus), white marlin (Tetrapturus albidus), and blue marlin (Makaira nigricans) in the western North Atlantic Ocean., Fishery Bulletin, Vol. 103 No. 4, pp. 588–600.

Malki, R., Masters, I., Williams, A.J., and Croft, T.N., (2014). Planning tidal stream turbine array layouts using a coupled blade element momentum--computational fluid dynamics model., Renewable Energy, Elsevier, Vol. 63, pp. 46–54.

Masters, I., Malki, R., Williams, A.J., and Croft, T.N., (2013). The influence of flow acceleration on tidal stream turbine wake dynamics: A numerical study using a coupled BEM--CFD model., Applied Mathematical Modelling, Elsevier, Vol. 37 No. 16, pp. 7905–7918.

McSherry, R., Grimwade, J., Jones, I., Mathias, S., Wells, A., and Mateus, A., (2011). 3D CFD modelling of tidal turbine performance with validation against laboratory experiments., 9th European Wave and Tidal Energy Conference.

Menter, F., (1993). Zonal two equation $κ$ $ω$- turbulence models for aerodynamic flows [C]., Orlando, USA.

Mycek, P., Gaurier, B., Germain, G., Pinon, G., and Rivoalen, E., (2013). Numerical and experimental study of the interaction between two marine current turbines., arXiv Preprint arXiv:1310.4921.

Pinon, G., Mycek, P., Germain, G., and Rivoalen, E., (2012). Numerical simulation of the wake of marine current turbines with a particle method., Renewable Energy, Elsevier, Vol. 46, pp. 111–126.

Rocha, P.A.C., Rocha, H.H.B., Carneiro, F.O.M., da Silva, M.E.V., and Bueno, A.V., (2014). k--$ω$ SST (shear stress transport) turbulence model calibration: A case study on a small scale horizontal axis wind turbine., Energy, Elsevier, Vol. 65, pp. 412–418.

Sfakiotakis, M., Lane, D.M., and Davies, J.B.C., (1999). Review of fish swimming modes for aquatic locomotion., IEEE Journal of Oceanic Engineering, IEEE, Vol. 24 No. 2, pp. 237–252.

Shi, W., Rosli, R., Atlar, M., Norman, R., Wang, D., and Yang, W., (2016). Hydrodynamic performance evaluation of a tidal turbine with leading-edge tubercles., Ocean Engineering, Elsevier, Vol. 117, pp. 246–253.

Shi, W., Wang, D., Atlar, M., Guo, B., and Seo, K., (2015). Optimal design of a thin-wall diffuser for performance improvement of a tidal energy system for an AUV., Ocean Engineering, Elsevier, Vol. 108, pp. 1–9.

Tedds, S.C., Owen, I., and Poole, R.J., (2014). Near-wake characteristics of a model horizontal axis tidal stream turbine., Renewable Energy, Elsevier, Vol. 63, pp. 222–235.

Tokić, G., and Yue, D.K.P., (2012). Optimal shape and motion of undulatory swimming organisms., Proceedings of the Royal Society of London B: Biological Sciences, The Royal Society, Vol. 279 No. 1740, pp. 3065–3074.

Wilcox, D.C., and others., (1998). Turbulence Modeling for CFD, Vol. 2, DCW industries La Canada, CA.

Wilga, C.D., and Lauder, G.V., (2001). Functional morphology of the pectoral fins in bamboo sharks, Chiloscyllium plagiosum: Benthic vs. pelagic station-holding., Journal of Morphology, Wiley Online Library, Vol. 249 No. 3, pp. 195–209.

Windsor, S.P., Norris, S.E., Cameron, S.M., Mallinson, G.D., and Montgomery, J.C., (2010). The flow fields involved in hydrodynamic imaging by blind Mexican cave fish (Astyanax fasciatus). Part II: gliding parallel to a wall., Journal of Experimental Biology, The Company of Biologists Ltd, Vol. 213 No. 22, pp. 3832–3842.

Yang, B., and Shu, X.W., (2012). Hydrofoil optimization and experimental validation in helical vertical axis turbine for power generation from marine current., Ocean Engineering, Elsevier, Vol. 42, pp. 35–46.

Zhou, C., Tan, M., Gu, N., Cao, Z., Wang, S., and Wang, L., (2008). The design and implementation of a biomimetic robot fish., International Journal of Advanced Robotic Systems, Vol. 5 No. 2, pp. 185–192.